Mathematical Biosciences and Engineering

MBE, 17(1): 286–308.
DOI: 10.3934/mbe.2020016
Received: 10 June 2019
Accepted: 26 September 2019
Published: 09 October 2019

http://www.aimspress.com/journal/MBE

Research article

Systematic analysis of single- and multi-reference adaptive filters for non-invasive fetal electrocardiography

Eleonora Sulas[1,*], Monica Urru[2], Roberto Tumbarello[2], Luigi Raffo[1] and Danilo Pani[1]

[1] Department of Electrical and Electronic Engineering, University of Cagliari, Cagliari 09123, Italy

[2] Division of Pediatric Cardiology, S. Michele Hospital, Cagliari 09123, Italy

* **Correspondence:** Email: eleonora.sulas@diee.unica.it; Tel: +390706755763; Fax: +390706755782.

Abstract: Non-invasive fetal electrocardiography (ECG) has been a research challenge for the past few decades. Due to instrumental noise and the spectral overlap of the maternal ECG signal, the signal-to-noise ratio for fetal ECG is very low. Various techniques have been proposed for cancelling the maternal ECG signal and extracting the fetal QRS complex from non-invasive abdominal recordings. Of these, adaptive filters enable satisfactory extraction when there is only a limited number of signal channels available, but the extraction quality is strongly dependent on the electrode placement. In this work, we systematically analyze this issue by comparing single- and multi-reference implementations of QRD-recursive least square (RLS) adaptive filters and evaluating their performances on real and simulated data in terms of the signal-to-interference ratio (SIR), maternal ECG attenuation, and fetal-QRS-complex detection accuracy. Beyond demonstrating the expected superior performance of the multi-reference version ($p < 0.05$) with respect to all metrics, except the QRS detection accuracy on synthetic data, we also analyze in detail the effectiveness of this technique with different lead orientations with respect to the correct interpretation of the adopted quality indexes. The results reveal that the single-reference approach, which is preferred when only the fetal heart rate is of interest, cannot produce a signal that has acceptable fetal QRS detection accuracy, regardless of the reference lead selection.

Keywords: adaptive filter; QRD-RLS; fetal ECG; electrocardiography; multi-reference; fetal heart rate; fetal monitoring; perinatal medicine

1. Introduction

Fetal cardiac monitoring in late pregnancy is mainly based on the analysis of changes in the fetal heart rate (fHR) [1,2] to determine whether the fetus is responsive to various physiological stimuli [1–3]. Finer studies of the variability of the fetal heart rate have demonstrated how this parameter relates to fetal development [4] and can be used to assess the proper functioning of the autonomic nervous system [5]. Ultrasound-based devices such as the cardiotocograph have been the primary choice for this purpose [6], whereas cardiac echocardiography is adopted for the assessment of fetal heart diseases [7]. In this context, fetal electrocardiography (fECG) enables access to very relevant information on fetal cardiac function, based on the electrical activation pattern of the fetal heart [6]. However, invasive techniques for this purpose, which record the fECG using a spiral scalp electrode, can only be used intrapartum, when membranes have already broken [2]. These techniques produce a signal of acceptable quality so they are currently adopted in clinical practice [8], even though they cannot be exploited for diagnostic purposes in early pregnancy, when in-utero treatments or birth scheduling can be considered [9]. Conversely, non-invasive fetal ECG (fECG) can be performed using a relatively comfortable and safe procedure at different gestational ages by applying surface electrodes to the maternal abdomen. However, the signal-to-noise ratio (SNR) for this procedure is low, due to the small size of the fetal heart, the feto-maternal compartments [10], maternal physiological interference, and instrumental noise [11]. Furthermore, fECG extraction from the interfering maternal ECG (mECG) is hampered by their spectral overlap so that, despite research efforts and the first devices having been introduced to the market, extracting a qualitatively effective non-invasive fECG remains an open research issue.

Several techniques for extracting the fECG from non-invasive recordings have been investigated in recent decades, including adaptive filtering, methods based on the wavelet transform, independent component analysis, principle component analysis, and soft computing tools like adaptive neural networks, genetic algorithms, and adaptive neuro-fuzzy inference systems [11]. Despite the superior performance demonstrated by blind-source separation techniques over that of adaptive filters for this specific problem [12], the latter can overcome the intrinsic limitations of the former, which requires a large number of channels (greater than eight, overall [13]). Considering reducing the number of electrodes applied on the maternal body is one of the constraints of this specific application, especially when required for unobtrusive wearable systems, adaptive filters can still be considered to be a valuable technique. Moreover, they can be naturally implemented in real time, which is not the case for several excellent blind-source separation methods, with some exceptions (e.g., [14,15]). Among the methods proposed in the literature, adaptive filters have been proposed by several authors who utilize different algorithms [16–22]. Originally, this approach was introduced by the authors of [16], whereby the adaptive filter received four chest ECG inputs to cancel the maternal component from a single abdominal lead. More recently, an adaptive filtering approach was proposed in the 2013 Physionet/Computing in Cardiology Challenge [23], wherein the dataset included only four abdominal channels per record. In [24], the authors cancelled the mECG from the recordings of four abdominal leads using an adaptive filter that received as references three out of four channels. The filter output was then subtracted from the channel and the filter coefficients were optimized to minimize the sum of the squares of this difference. A Wiener-filter-like method was then adopted to compute the filter coefficients. Behar et al. [20] compared an echo-state neural-network-based filtering approach to a least mean square filter, recursive least square (RLS)

adaptive filter, and template subtraction techniques. The first performed slightly better than the others but the improvement was not statistically significant. Non-invasive fECG extraction has also been investigated by combining methods, for example, using multi-stage adaptive filters [21] or adaptive filters and wavelet transform [25].

The drawback of adaptive filtering using a reduced number of leads (in principle one thoracic and one abdominal) is the strong dependency of the output quality on the electrode placement, since the reference mECG lead must be morphologically similar to the mECG projection contaminating the fECG in the abdominal leads. This problem could be solved by using multiple non-coplanar thoracic leads to roughly reconstruct the mECG morphology in any abdominal lead. The multi-reference approach has been investigated using different adaptive filtering methods [22] but there has yet to be an in-depth methodological analysis that can answer the following important questions: Is it worthwhile to use multiple mECG reference leads rather than a single lead when dealing with real non-invasive fECG recordings? Or, alternatively, to what extent can a single-reference adaptive filter provide adequate mECG attenuation, at least on abdominal leads parallel to the reference lead? When only the fHR is needed, is it effective to adopt the single-reference approach? The answer to these questions is relevant for guiding the selection of the appropriate technique for a given problem.

To answer the above questions, in this work, we analyzed the performance of a prototypical multi-reference (MR) adaptive filter, i.e., QR decomposition with back-substitution recursive least-squares (QRD-RLS), which we chose for its numerical stability and good performance. Its performance was compared to its single-reference (SR) variant by cancelling the mECG on abdominal leads having different spatial orientations. The assessment was performed on a large dataset comprising real recordings acquired on 20 pregnant women within the framework of the non-invasive fetal ECG analysis (NInFEA) project of the University of Cagliari, and on synthetic signals generated by the FECGSYN toolbox [26]. The real dataset contained a total of 112 non-invasive fECG signal channels, and the synthetic dataset contained a total of 400 channels. These datasets enabled an in-depth analysis of the results, which were found to subvert some common-sense beliefs regarding the use of SR adaptive filters in this specific application.

2. Materials and method

2.1. Adopted dataset

To perform some of the analyses required for comparing the SR and MR QRD-RLS adaptive filters, we used a custom dataset. This was necessary because of the lack of available datasets featuring the required representative leads. In this section, we describe the real and synthetic datasets used in the performance analysis.

2.1.1. Real dataset

The real dataset is composed of biopotentials acquired from healthy pregnant women. Along with the electrophysiological signals, a simultaneous cardiac pulsed-wave doppler (PWD) trace was recorded. In this work, this dataset played the main role in providing ground truth for the fetal heart activity from a mechanical perspective, which was important for confirming the presence of fetal

QRS complexes. The PWD traces were acquired using a Philips iE33 Ultrasound Machine (Philips, The Netherlands), as described in [27]. The biopotentials were recorded with a Porti7 portable physiological measurement system (TMSi, The Netherlands) at 2048 Hz and 22–bit resolution. No high-pass filtering was performed, and the actual bandwidth was limited by a digital decimation filter with a cut-off frequency of approximately 550 Hz. Bipolar channels, which were used on the thorax, enabled differential measurements, whereas unipolar channels connected to electrodes placed on the abdomen measured the biopotential of one electrode with respect to the average of all the unipolar electrodes in use. Figure 1 shows the positions of the electrodes on the maternal body.

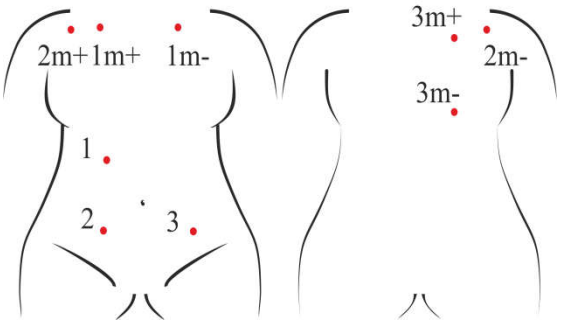

Figure 1. Electrode positions: the m channels are the bipolar maternal leads, whereas the unipolar channels are on the abdomen.

The chosen configuration included six electrodes for three bipolar channels that captured three non-coplanar maternal leads on the chest and three abdominal electrodes to obtain three digital abdominal bipolar leads and one unipolar lead. A ground electrode was placed on the right hip. Figure 2 shows a sample trace acquired using this setup.

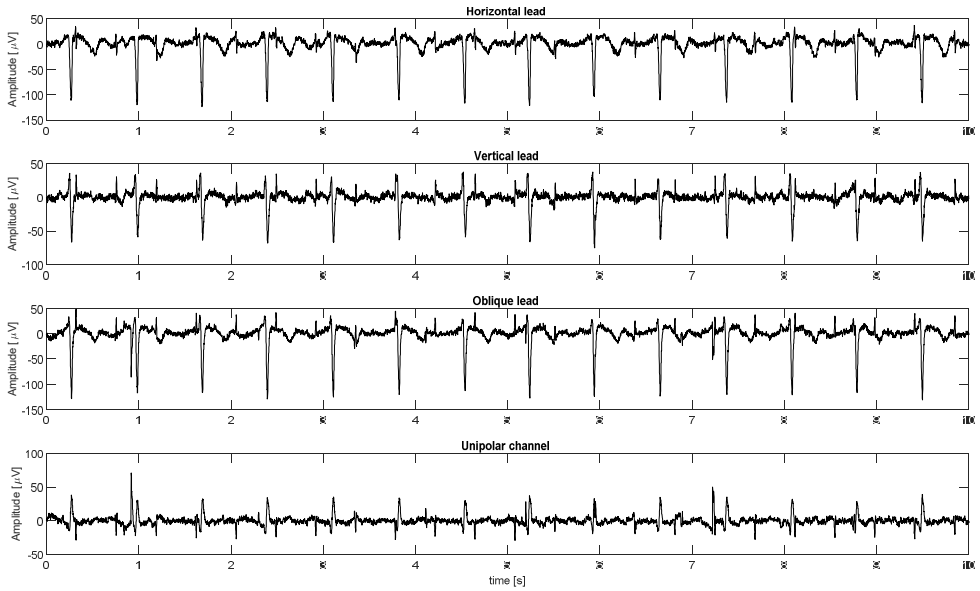

Figure 2. A sample signal from the real dataset.

Figure 3 shows an example of the simultaneous recording of PWD traces and electrophysiological signals. The specific heart projection adopted for this dataset for ultrasound recording was the five-chamber apical window, which allows inspection of the flows across the mitral and aortic valves.

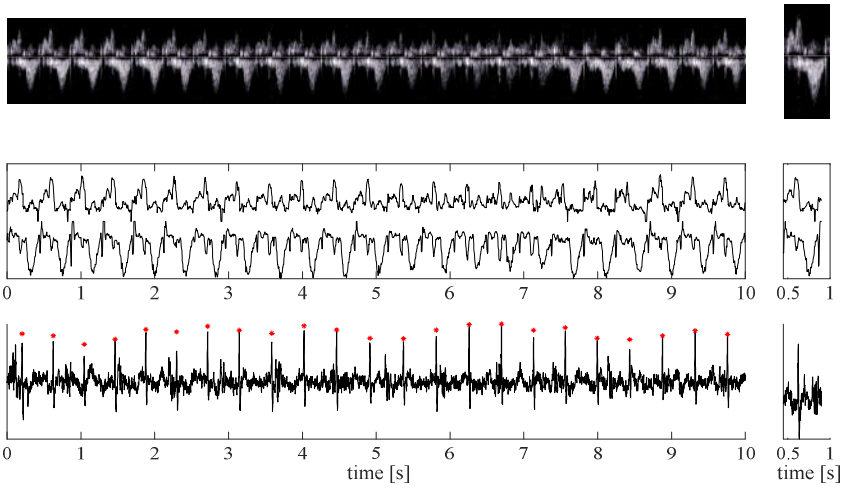

Figure 3. Example of a simultaneous PWD trace (top), its upper and lower envelopes (middle) and the fECG lead obtained by QRD-RSL adaptive filtering (bottom), with marked fetal QRS complexes. On the right, zoom-in signals of a single cardiac cycle.

The dataset included 28 multichannel signals from 20 healthy pregnant women between the 21st and the 27th weeks of gestation with healthy fetuses (for a total of 112 abdominal channels leading to as many non-invasive fECG signals). The gestational epoch was selected to ensure the best morphological accuracy of the transabdominal signals and to limit the influence of the vernix caseosa, which is characterized by the lowest conductivity of the anatomical layers surrounding the fetus [10]. The signal duration was fixed to ten seconds, similar to the standard resting ECG. Recording was performed at the Division of Pediatric Cardiology of the S. Michele Hospital (Cagliari, Italy). The study was approved by the Independent Ethical Committee of the Cagliari University Hospital (AOU Cagliari) and was performed according to the principles outlined in the Helsinki Declaration of 1975, as revised in 2000. All the volunteers provided their signed informed consent to the protocol.

2.1.2. Synthetic dataset

The FECGSYN tool [26,28] is a reference open-source platform for non-invasive fetal electrocardiography research[1]. In abdominal fECG recordings, surface electrodes measure the electrical potential created by cardiac sources (i.e., maternal and fetal myocardia) and noise sources (e.g., muscle activity from movement or contractions), which propagate throughout the volume conductor. The FECGSYN simulator considers all of these potentials to be point dipoles that can be rotated and translated. These dipoles have two basic attributes: a vector represented by three coordinates in the Cartesian coordinate system and a location, which, together with the electrode

[1]Available at http://fernandoandreotti.github.io/fecgsyn/

locations, defines a matrix of the signals propagated to the observation points. To project the ECG signals, we used a projection matrix built using the cardiac dipole model. This projection matrix contains information about the permittivity of the conductor (assumed constant), dipole origin, and relative location between the observing electrodes and the source [28].

By exploiting this principle, FECGSYN is able to generate maternal–fetal ECG mixtures with a realistic amplitude, morphology, beat-to-beat variability, and heart rate changes and noise [26]. Movements (rotations and translations) of fetal and maternal hearts due to respiration, fetal activity, and uterine contractions can also be considered by the simulator. In this work, the fECG mixtures were generated at 2048 Hz with a duration of 10 s. To the clean signals, we added realistic motion artifacts, electrode movements, and baseline wandering. The electrodes were placed as shown in Figure 4, which was also the reference position for the real recordings. Figure 5 shows an example of the synthetic signals generated specifically for this purpose.

The cardiac and noise signals were calibrated with respect to the maternal signal, for which we chose the SNR of the fECG relative to the mECG (SNR_{fm}), i.e., –18 dB, and the SNR of the mECG relative to noise (SNR_{mn}). We reproduced five SNR_{mn} values (3 dB, 5 dB, 9 dB, 12 dB, and 15 dB). The maternal and fetal HRs were assumed to be fixed at 90 bpm and 150 bpm, respectively. For each SNR_{mn}, we simulated 20 slightly different fetal heart positions. As such, one hundred virtual subjects were created, each of which included four abdominal signals (Figure 4), i.e., the horizontal (1–2), vertical (1–3), and oblique (1–4) leads and a unipolar channel (4), for a total of four hundred synthetic abdominal signals. For each of these, we also created three non-coplanar thoracic leads (5–6, 5–7, and 7–8).

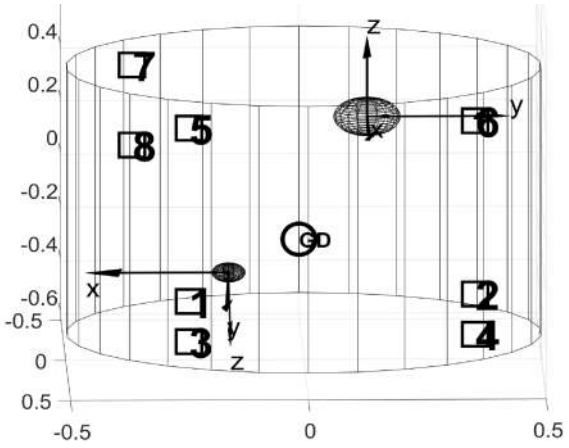

Figure 4. Graphical representation illustrating the locations of the maternal heart (upper circle) and the fetal heart (lower circle). Squares, located on the maternal abdomen, indicate the electrode positions and are numbered according to the corresponding output channel. The reference electrode is labelled GD (middle circle).

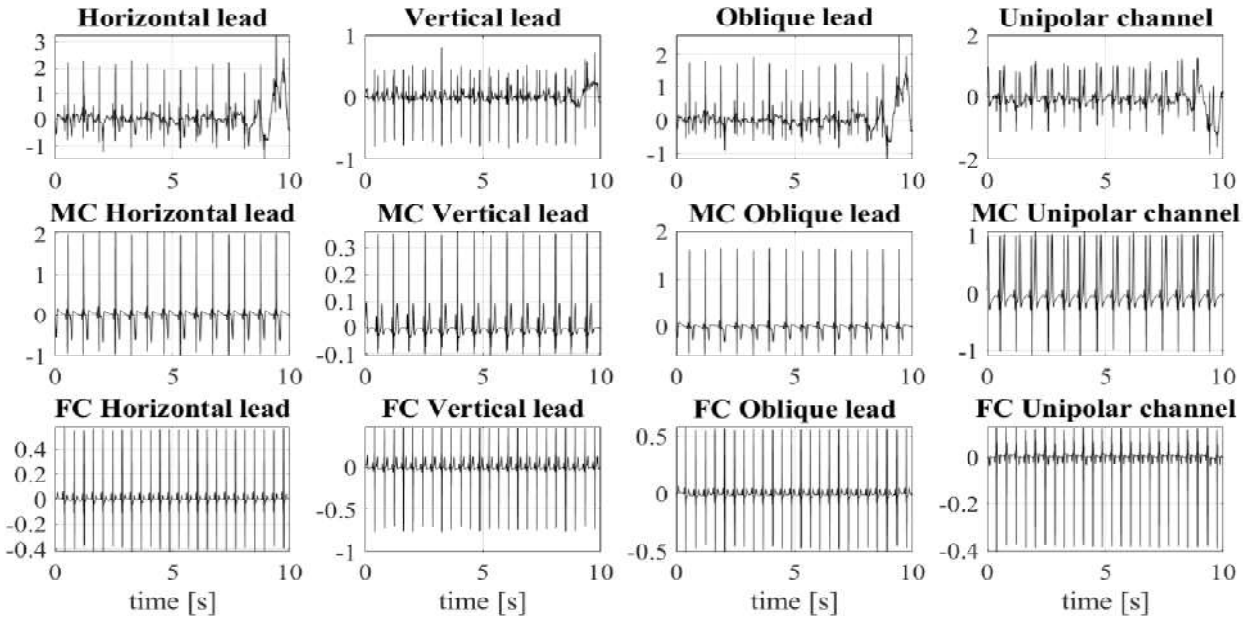

Figure 5. The first row shows the simulated signals of the horizontal, vertical, oblique, and unipolar channels. The second and third rows, labelled MC and FC, respectively, show the associated mECG and fECG components.

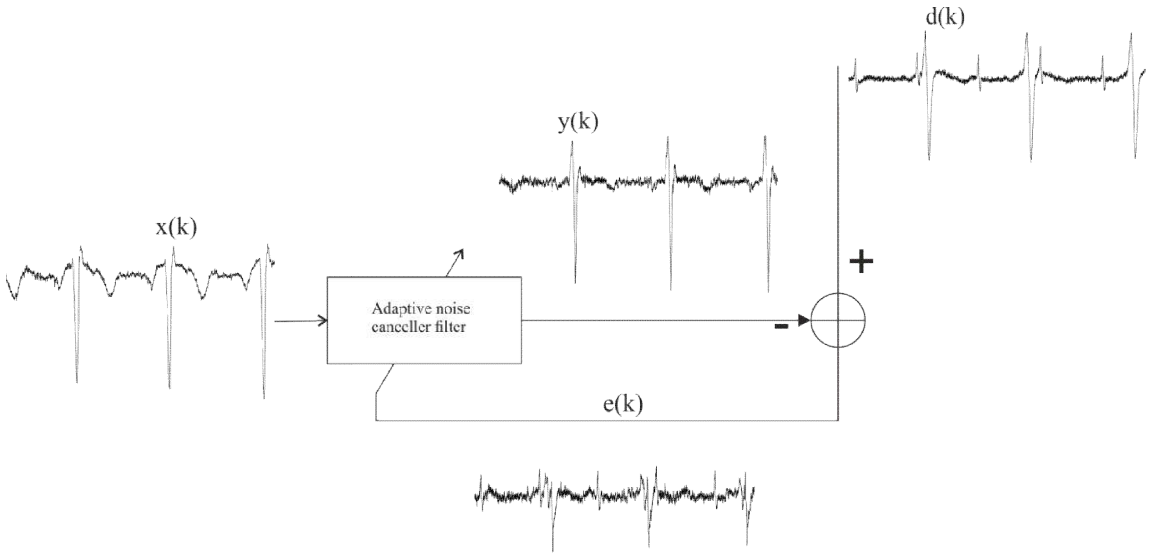

Figure 6. Schematic diagram of single-reference adaptive filter used as an adaptive noise canceller, applied to the non-invasive fECG extraction problem to remove the mECG contribution from abdominal signals.

2.2. MECG cancellation by RLS adaptive filter

Generally speaking, an adaptive filter is a self-modifying digital filter that adjusts its coefficients to minimize the error function, which is the distance between the reference signal and the output of

the adaptive filter [29]. The adaptive filter can be used in different configurations, one of which is the adaptive noise canceler, whose block diagram is presented in Figure 6, which we adapted to the non-invasive fECG extraction problem. Generally speaking, it is used to extract a clean version of the signal of interest *s(k)*, which is characterized by an additive noise component *n(k)*. The reference signal must be strongly correlated with *n(k)* but not *s(k)*. The adaptive filter adjusts its coefficients to obtain an output *y(k)* that approximates *n(k)*, thereby forcing the error signal *e(k)* to resemble *s(k)*. The adaptation of the filter coefficients follows the minimization process of a particular cost function. With reference to Figure 6, where *d(k)* is the recorded abdominal signal, *x(k)* is the reference maternal lead, *y(k)* is the maternal component of the abdominal signal reconstructed by the filter, and *e(k)* is the extracted fECG.

$$\mathrm{d(k)} = \mathrm{s(k)} + \mathrm{n(k)} \tag{1}$$

$$\mathrm{x(k)} \cong \mathrm{n(k)} \tag{2}$$

$$\mathrm{y(k)} = \mathrm{w^T x(k)} \tag{3}$$

$$\mathrm{e(k)} \cong \mathrm{s(k)} \tag{4}$$

From the equations above, we can better understand the effect of the adaptive noise canceler when applied to the fECG extraction problem. The *d(k)* signal is a combination of the noise and the signal of interest. The maternal lead *x(k)* approximates the noise, and *y(k)* is the filter output that has been optimized to mimic the maternal component obtained by the abdominal lead by the use of reference signal *x(k).* Finally, *e(k)* is our signal of interest. Compared to other methods, RLS adaptive filters pay for their faster convergence with a higher computational complexity. Moreover, their direct matrix inversion operations may cause numerical stability problems. To address this problem, QRD-RLS filters have been introduced [30], which exhibit both fast convergence and numerical stability. For this reason, we chose the QRD-RLS adaptive filter as the prototypical adaptive filter for this study.

The RLS filter family uses the weighted least-squares objective function, which is defined as follows:

$$\xi_{\mathrm{D}}(\mathrm{k}) = \sum_{\mathrm{i}=0}^{\mathrm{k}} \lambda^{\mathrm{k}-1}[\mathrm{d(i)} - \mathrm{w^T x(i)}]^2 = \mathrm{e^T(k)e(k)} \tag{5}$$

In this equation, e(k) is defined as follows:

$$\mathrm{e(k)} = \begin{bmatrix} \mathrm{d(k)} \\ \lambda^{1/2}\mathrm{d(k-1)} \\ \vdots \\ \lambda^{\mathrm{k}/2}\mathrm{d(0)} \end{bmatrix} - \begin{bmatrix} \mathrm{x_P^T} \\ \lambda^{1/2}\mathrm{x_P^T(k-1)} \\ \vdots \\ \lambda^{\mathrm{k}/2}\mathrm{x_P^T(0)} \end{bmatrix} \mathrm{w_P(k)} = \mathrm{d(k)} - \mathrm{x_P(k)w_P(k)} \tag{6}$$

$$\mathrm{x_P^T(k)} = \left[\mathrm{x_k^T}\ \mathrm{x_{k-1}^T} \ldots \mathrm{x_{k-N+1}^T}\right] \tag{7}$$

and N is the number of filter coefficients. The forgetting factor λ, which ranges from 0 to 1, allows the most recent error samples to be emphasized. If we define the *R* and *p* parameters, introducing the forgetting factor λ:

$$R(k) = \sum_{i=0}^{k} \lambda^{k-1} x(i)x^T(i) = X^T(k)X(k) \tag{8}$$

$$p(k) = \sum_{i=0}^{k} \lambda^{k-1} d(i)x(i) = X^T(k)d(k) \tag{9}$$

then the optimum solution takes the following form:

$$w(k) = R^{-1}(k)[x(k)e(k) + R(k)w(k-1)] \tag{10}$$

where the computation of the inverse matrix of R can lead to an ill-conditioned problem. The convergence rate, misalignment, and numerical stability of adaptive algorithms depend on the condition number of the input signal covariance matrix. The higher is this condition number, the slower is the convergence rate and/or the more unstable is the algorithm.

2.2.1. QR decomposition

An alternative RLS implementation is based on QR decomposition, which involves the triangularization of the input data matrix. QR decomposition is numerically stable and solves the instability problem of the RLS implementation. We note that matrix $X(k)$ is $(k+1)\times(N+1)$, which means that its order increases as the iterations progress. The QR-decomposition process applies an orthogonal matrix $Q(k)$ of order $(k+1)\times(k+1)$ to transform $X(k)$ into a triangular matrix $U(k)$ of order $(N+1)\times(N+1)$ such that:

$$Q(k)X(k) = \begin{bmatrix} O \\ U(k) \end{bmatrix} \tag{11}$$

where O is a null matrix of order $(k-N)\times(N+1)$. Matrix $Q(k)$ indicates the overall triangularization process and may be implemented in different ways, such as the numerically well-conditioned Givens rotations or the Householder transformation [31]. The vector $e_q(k)$ is expressed as follows:

$$e_q(k) = Q_P(k)e(k) = \begin{bmatrix} e_{q1}(k) \\ e_{q2}(k) \end{bmatrix} = \begin{bmatrix} d_{q1}(k) \\ d_{q2}(k) \end{bmatrix} - \begin{bmatrix} 0 \\ U_P(k) \end{bmatrix} w_P(k) \tag{12}$$

Minimizing $\|e_q(k)\|^2$ or the cost function $\xi_D(k)$ is equivalent. Therefore, Eq. (5) is minimized by choosing the $w_P(k)$ in Eq (12) such that $d_{q2}(k) - U_P(k)w_P(k) = 0$ [31].

2.2.2. Single- and MR QRD-RLS adaptive filters

The theory presented thus far was conceived for the SR implementation of the QRD-RLS adaptive filter. In a MR implementation, there are multiple reference signals that meet the definition of noise (Figure 7). If M is the number of channels, which in our case is equal to three, i.e., the number of non-coplanar bipolar thoracic leads (x1, x2, and x3 in Figure 7), $N_1, N_2, \ldots, N_M$ is the number of taps for each of the M filters. In our approach, in a sample, we shift from each channel one at a time and progress recursively from the first to last channel. In this work, we implemented the filtering routines provided in [31] and adapted them to this problem.

For the specific application, we chose the first thoracic lead (1 m in Figure 1 for the real dataset and 5–6 in Figure 4 for the synthetic one), which is perpendicular to the sagittal plane, to be the input reference for the SR technique, whereas we used all three thoracic leads (1 m, 2 m, and 3 m in Figure 1 for the real dataset and 5–6, 5–7, and 7–8 in Figure 4 for the synthetic one) for the MR version. Moreover, adaptive filters require proper tuning of their parameters to achieve the best compromise

between performance and computational cost [20]. In the RLS implementation, there are two important parameters: the forgetting factor λ and the number of taps N. In both implementations, we set λ to 0.999 and N to 20 (for each of the three channels in the MR implementation). We optimized both these parameters in the training phase on the real dataset. We note that other studies have obtained the same values following similar procedures [20].

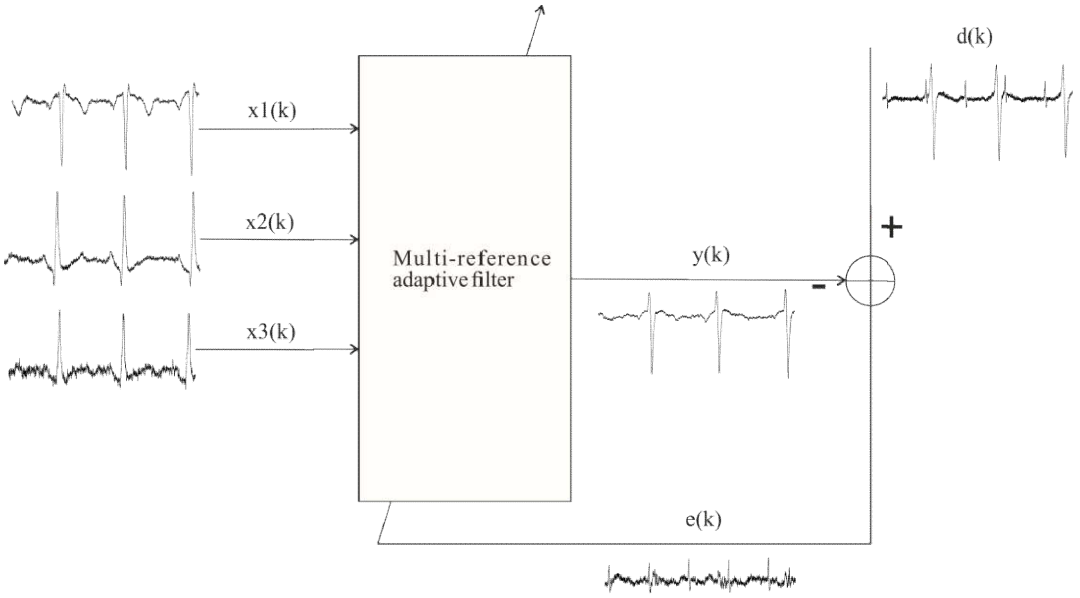

Figure 7. Block diagram of the multi-reference QRD-RLS adaptive filter used as adaptive noise canceller, applied to the non-invasive fECG extraction problem to remove the mECG contribution from the abdominal signals.

2.2.3. Signal pre-processing

Baseline wandering, especially when no high-pass filtering occurs in the analog signal acquisition chain, cannot be addressed by the adaptive filter in the real dataset. In fact, several factors contribute to its generation, from maternal breathing to fetal and cable movements, which have different reflections on different leads, even more so on the abdominal leads. To address this, a simple pre-processing step is usually recommended prior to fECG extraction. As proved in [20], the cut-off frequency of the high-pass filter should be higher than that imposed by the current guidelines, which is 0.67 Hz [32], mainly to compensate for such a stronger baseline wandering. To preserve the low-frequency components of the ECG, which are mainly related to P and T and to the ST segments, the signal was high-pass filtered only at 1 Hz by a bidirectional implementation of an equiripple finite impulse response (FIR) filter of 1124–th order.

2.3. Comparative analysis methods

In principle, the availability of three non-coplanar leads for the mECG should enable projection of the maternal heart vector in any lead direction. Obviously, by providing more information for the maternal heart vector than is possible with a single projection in a given direction, the MR

QRD-RLS filter should outperform its SR counterpart. However, a proper selection of the abdominal lead parallel to the maternal chest lead used as reference could be expected to produce acceptable results, at least with respect to the fHR computation. Since a reduction in the number of processing leads is important in the context of this application, especially for wearable monitoring systems, this assumption must be carefully verified. For instance, currently available wearable non-invasive fECG monitors, such as the Monica Novii Wireless Patch System (Monica Healthcare, Nottingham, UK) and Nemo Fetal Monitoring System (Nemo Healthcare, Veldhoven, The Netherlands), use only five and six electrodes, respectively. More recently, Imec and BloomLife showcased a fetal ECG and mobile wearable monitoring device featuring the first integrated circuit produced for this reason, which uses only five channels.

Because in this study we focused on evaluating the extraction of the maternal component, to perform this analysis, we adopted the following metrics:

a. The signal-to-interference ratio (SIR), which is more appropriate than SNR when the noise is a well-defined interference superimposed onto the signal of interest;

b. mECG attenuation after adaptive filtering, to enable better quantify how much of the maternal ECG is removed from the abdominal leads;

c. Fetal QRS peak detection accuracy, since fHR is the simplest parameter that can be extracted from the fECG.

SIR is often used to analyze the power in both the enhanced and rejected signal sources, for example when blind-source separation algorithms are benchmarked [19]. Since in this case the signal of interest was the fECG, whereas the interference was the mECG, the SIR was computed as follows:

$$SIR_{dB} = 20 * log_{10}(\frac{App_f}{App_m}) \tag{13}$$

where App_m is the peak-to-peak amplitude of the maternal average QRS complex and App_f is the peak-to-peak amplitude of the average fetal QRS complex. Since the primary aim of using an adaptive filter with thoracic references is the removal of maternal ECG interference from the abdominal leads, the SIR parameter quantifies this cancellation process more effectively than other performance metrics. In Eq (13), the authors computed the peak-to-peak amplitudes based on the average QRS complex for both the fECG and mECG, because the local variability due to noise and small movements influences this computation. In this study, we annotated the fetal QRS complexes with the help of the simultaneous PWD signal, whereas we detected the maternal QRS using the Pan-Tompkins algorithm [33] on the horizontal chest lead.

To obtain a significant SIR, we performed QRS averaging only between complexes exhibiting a maximum of cross-correlation, based on the Pearson's correlation coefficient above a given threshold, which was chosen empirically to be equal to 0.6 to take into account the presence of noise. We set the time window for the fetal-QRS-complex template to 40 ms, as reported in [34], and that for the maternal QRS complex to 100 ms [35]. If fewer than four QRS complexes were recognized as being similar to the output signal, based on their cross-correlation values that signal (either fECG or mECG) could be treated as non-deterministic. In such an event, in Eq (13), the authors substituted the App peak-to-peak amplitude of the signal with four times its standard deviation, thus treating the signal as non-deterministic. Regarding the mECG, this situation occurs due to its adequate suppression, whereas for the fECG, it occurs due to the fact that fECG is not detectable on that lead.

By definition, the SIR is influenced by the amplitude of the signal and interference. The fECG

amplitude depends on the fetal presentation, the developmental stage, and the composition of the feto-maternal compartment tissues. For this reason, we also computed the SIR on the raw signal to evaluate the performances of the SR and MR techniques by comparing their SIR values before and after applying the adaptive filter.

A high SIR implies good mECG cancellation from the abdominal recordings, whereas a low SIR indicates a trace in which the mECG signal power is still high, which means the maternal amplitudes are still significant in the processed signal with respect to the fECG. To enable quantification of the mECG removal, regardless of the fECG amplitude, we also computed the attenuation of the mECG as follows:

$$Attenuation = -20log_{10}\left(\frac{App_{out}}{App_{in}}\right) \tag{14}$$

where App_{out} is the peak-to-peak amplitude of the average maternal QRS complex in the processed abdominal signal and App_{in} is the peak-to-peak amplitude of the average maternal QRS complex in the original (unprocessed) abdominal lead.

Moreover, since the SIR is inherently influenced by both the fetal and maternal QRS amplitudes, to decouple these aspects, we evaluated both the fetal and maternal QRS amplitudes (in the original abdominal leads and in their SR and MR processed leads).

Finally, we used the *jqrs* fetal QRS detector [36] on all the processed abdominal leads to obtain the fHR. This algorithm consists of a window-based peak energy detector based on adaptive thresholding and forward and backward searches. We chose this algorithm from the fetal QRS detectors available in the scientific literature because it performed better in the training phase than others on fECG traces that have a very low SNR . The accuracy (Acc) of the peak detector for all the signals was computed as follows:

$$Acc = (TP + TN)/(TP + TN + FP + FN) \tag{16}$$

where TP is the number of true positive detections, TN is the number of true negatives, FP is the number of false positives, and FN is the number of false negatives.

All the processing was performed in Matlab. To represent the metrics that provided some hints about the actual shape of their distributions, we selected the box-and-whiskers plot. In this plot, the median is highlighted, the box indicates the 25th and 75th percentiles, and the whiskers extend to the most extreme data points that are not considered to be outliers. Furthermore, we performed a statistical analysis to investigate the significance of the differences between the SR and MR results in terms of SIR, mECG attenuation, and fetal QRS detector accuracy. To do so, we considered the abdominal leads separately. First, we used the Lilliefors test to check the normality of the distributions. If the result does not satisfy the assumption of normal distribution, a non-parametric statistical test was adopted to determine the significance of the results. In particular, we chose the Wilcoxon signed rank test, considering a significance level $p < 0.05$.

3. Results and discussion

In Figures 8–10 and Table 1, we grouped the results for the original (raw, OR) abdominal channels (i.e., the unfiltered ones) and the SR and MR processed leads, respectively, for the horizontal (hor), vertical (ver), oblique (obl), and unipolar (unip) abdominal leads. In these

figures, the distributions of the results are shown as boxplots to provide a visual representation of the results, and the table shows the median and first and third quartile values of all the distributions.

First, we compare the performances of the SR and MR methods, and later our focus shifts to compare the different leads.

Figure 8 shows the overall results for the real dataset. We can see that the SIR values always show an improvement with respect to the raw signal, regardless of the channel or the chosen approach, but the MR adaptive filter significantly outperforms the SR ($p < 0.0009$). Remarkably, the significantly poor performance of the SR adaptive filter was confirmed when we considered the horizontal abdominal lead, even though the reference and processed leads were in parallel positions. Similar results were obtained for the SIR, as shown in Figure 9 for the synthetic dataset ($p < 0.0002$). By evaluating the mECG attenuation, it was possible to see how the MR approach significantly outperformed the SR implementation again ($p < 0.0001$), whichever lead was used.

Figures 8 and 9 also show the fetal and maternal QRS amplitudes, respectively, for the real and synthetic datasets. It is clear that the values of these two parameters decreased after adaptive filtering. Since we determined that the reference signals were not correlated with the fECG, because they were acquired on the upper part of the chest, the fECG attenuation can only be ascribed to both the frequency behavior of the filter and to a rough estimation of the fetal QRS amplitude on the original abdominal leads due to the larger maternal contributions. Moreover, the results for the fetal QRS amplitude in the real dataset reveal that the adoption of a differential measurement in the real recordings helped to increase the fECG amplitude from that of a unipolar lead (Figure 8). In fact, the median OR fetal amplitude values for the horizontal and oblique leads are higher than those of the unipolar channel. The differences between the distributions of these values are statistically significant ($p = 0.004$ for horizontal vs. unipolar, $p = 0.001$ for oblique vs. unipolar). This was also observed by the authors of [37], along with a reduction in the common-mode interference. The opposite behavior observed on the synthetic dataset (Figure 9) could lead to wrong conclusions. In fact, on synthetic signals, differential measurements generated reductions in the signals of both the fetal and maternal ECGs. This effect can be seen in Figure 11, which shows an example of the output synthetic signals.

Moreover, by looking at the SIR of the raw (OR) synthetic signals, it is clear that the lower values of the bipolar leads are comparable to those of the unipolar channel. Furthermore, both the fECG and the mECG are significantly smaller overall on the vertical lead, which is also evident in Figure 5. Moreover, the maternal amplitude was lower than the fECG amplitude, despite having set the SNR_{fm} to −18 dB for the generation of the unipolar channels (from which the differential measurements were taken) to decrease this effect. In the real dataset, this never occurred, which suggests the need to be very careful when using a synthetic dataset for analyzing the performance of a fECG extraction algorithm.

Finally, on the real dataset, the accuracy of the fetal QRS detection (Figure 10, left) was significantly higher for the MR version of the adaptive filter than the SR version ($p < 0.004$). Moreover, the accuracy of the fetal QRS detection obtained from the SR output reveals the unreliability of this approach and strongly depends on the fECG amplitude. However, the difference between the two techniques (MR and SR) vanishes on the synthetic dataset (Figure 10, right, $p < 0.8$), because of the easy detectability of the synthetic fetal QRS from such signals,

which is far from the reality.

To summarize the above findings, we performed a statistical analysis by the Wilcoxon test to enable a comparison of the MR and SR adaptive filters in terms of SIR. Tables 2 and 3 show the maternal attenuation and fetal QRS detection results on the separate channels for the real and synthetic datasets, respectively.

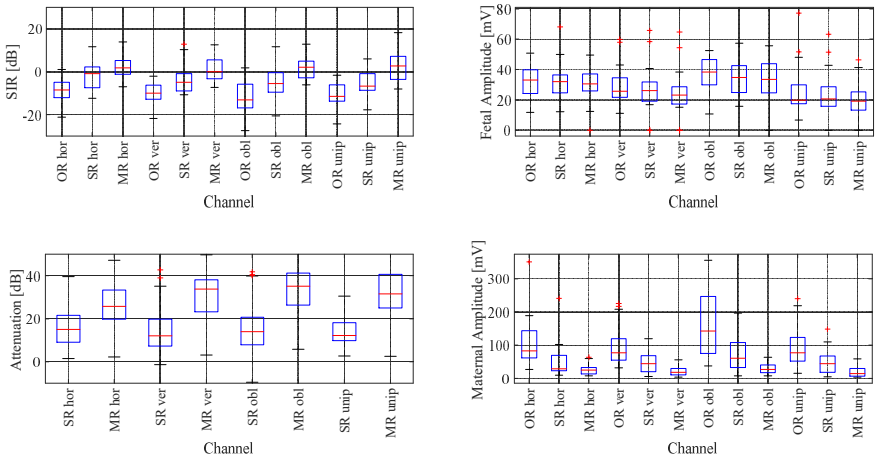

Figure 8. Results from real dataset. OR: Original raw abdominal lead, SR: Single-reference method, MR: Multi-reference method, hor: Horizontal lead, ver: Vertical lead, obl: Oblique lead, unip: Unipolar channel.

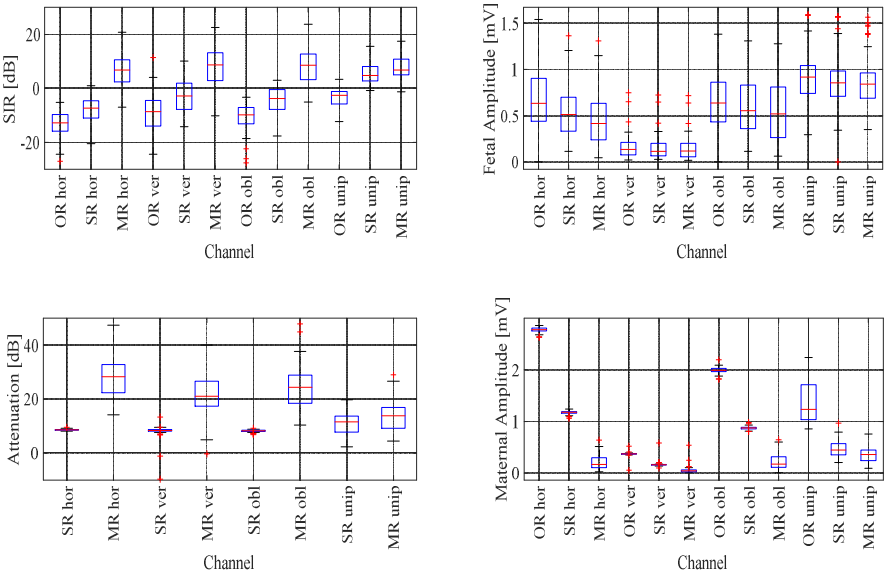

Figure 9. Results from the synthetic dataset. OR: Original raw abdominal lead, SR: Single-reference method, MR: Multi-reference method, hor: Horizontal lead, ver: Vertical lead, obl: Oblique lead, unip: Unipolar channel.

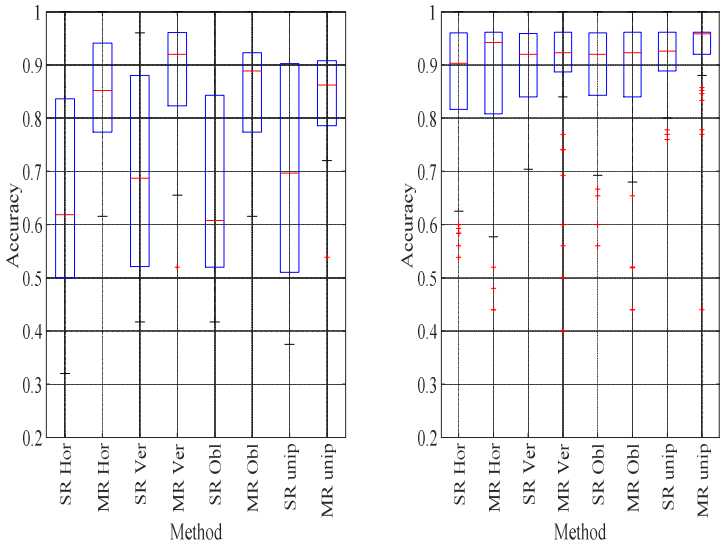

Figure 10. Accuracy of the fetal QRS detector applied to the output signals from SR and MR QRD-RSL algorithms, for real (left) and synthetic (right) datasets.

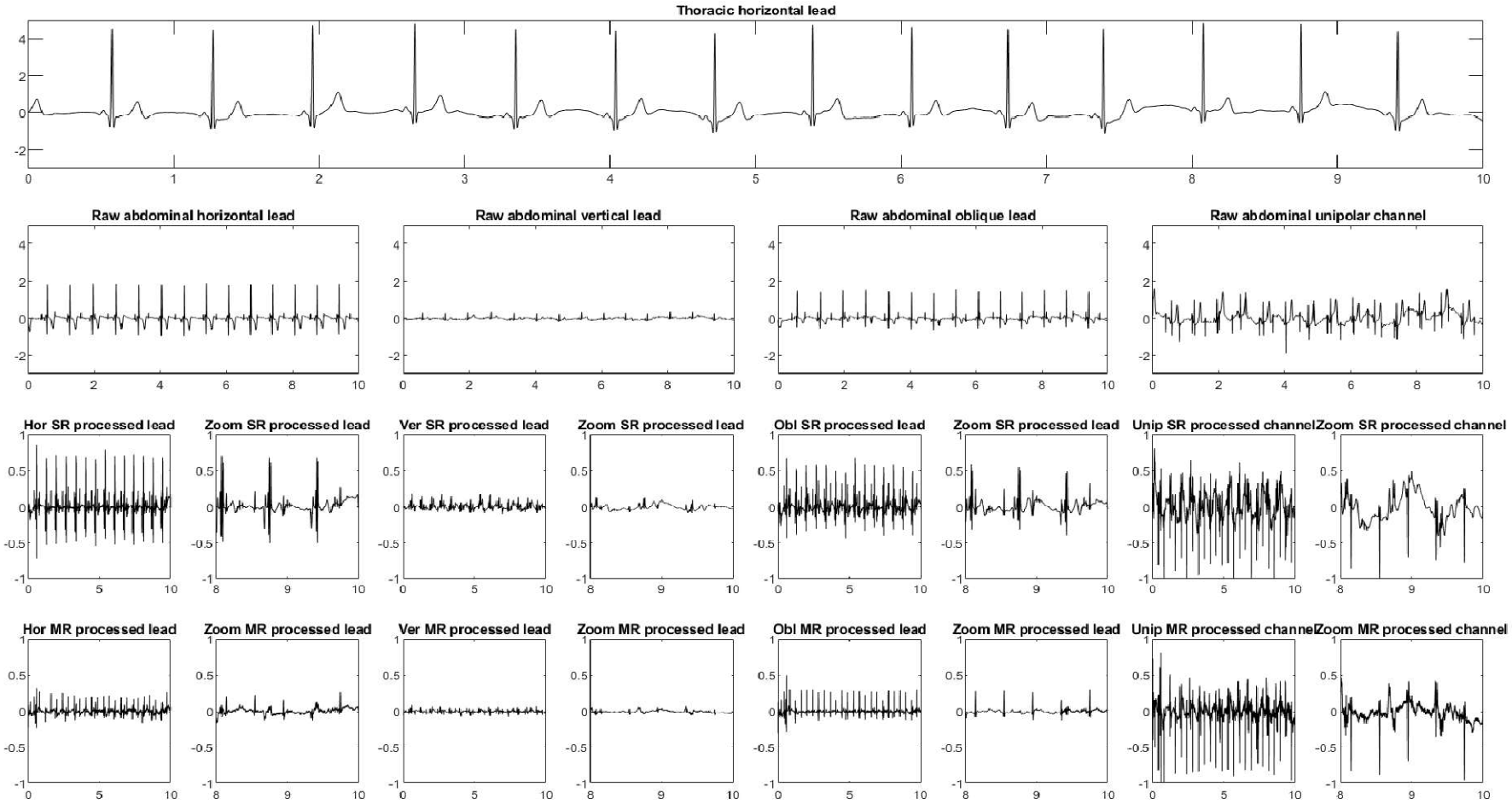

Figure 11. Synthetic dataset: raw thoracic lead and raw and processed abdominal leads at different zoom levels for a single subject. In detail: (i) the first row shows the thoracic horizontal maternal lead used as reference in the SR implementation; (ii) in the second row, there are the four raw leads in the order: horizontal, vertical, and oblique leads and the unipolar channel; (iii) in the third row, these signals are respectively processed using the SR method and each is plotted with its respective zoom: (iv) the last row shows the processed signals by the MR technique and their zooms.

Table 1. Real and synthetic dataset results: median values (first quartile, third quartile).

		SIR [dB]	Fetal Amp [μV]	matAmp [μV]	matAtt [dB]	QRSdetAcc
Real dataset results	OR hor	-8.5(-12.09 -4.97)	33.17(24.18 39.89)	83.37(62.20 144.04)		
	SR hor	-0.87(-7.39 2.23)	32.14(24.61 36.42)	28.97(23.00 69.61)	15.02(9.11 21.50)	0.62(0.50 0.84)
	MR hor	1.79(-1.20 5.17)	30.61(25.83 37.10)	24.75(13.71 32.91)	25.75(19.80 33.41)	0.85(0.77 0.94)
	OR ver	-9.92(-12.79 -6.26)	25.7(21.64 34.56)	77.6(54.84 119.37)		
	SR ver	-4.85(-8.91 -0.93)	26.13(19.26 31.89)	44.17(20.26 68.48)	12.08(7.32 19.76)	0.69(0.52 0.88)
	MR ver	-0.06(-3.26 5.46)	23.14(17.33 28.57)	18.55(10.59 30.33)	33.79(23.17 38.06)	0.92(0.82 0.96)
	OR obl	-13.05(-16.88 -5-76)	38.45(29.91 46.66)	142.47(74.90 246.37)		
	SR obl	-5.48(-9.50 -0.39)	34.81(24.95 42.67)	60.68(33.25 107.82)	13.99(7.88 20.71)	0.61(0.52 0.84)
	MR obl	2.03(-2.78 4.92)	33.46(24.63 43.78)	27.38(17.92 40.94)	35.09(26.38 41.31)	0.89(0.77 0.92)
	OR unip	-11.4(-13.72 -6.11)	19.84(17.48 29.82)	76.86(51.94 123.54)		
	SR unip	-6.72(-8.60 -0.89)	20.71(15.74 28.58)	43.95(18.24 67.64)	12.16(9.86 18.20)	0.7(0.51 0.90)
	MR unip	2.63(-3.63 7.11)	19.11(13.19 25.23)	14.52(7.10 30.39)	31.5(24.98 40.63)	0.86(0.79 0.91)
Synthetic dataset results	OR hor	-12.8(-9.71 -15.84)	0.63(0.44 0.90)	2.78(2.75 2.81)		
	SR hor	-7.32(-11.03 -4.59)	0.51(0.33 0.70)	1.18(1.16 1.19)	8.57(8.46 8.78)	0.9(0.82 0.96)
	MR hor	6.8(2.42 10.53)	0.42(0.24 0.63)	0.17(0.10 0.30)	28.25(22.41 32.79)	0.94(0.81 0.96)
	OR ver	-8.61(-13.90 -4.50)	0.14(0.08 0.21)	0.37(0.37 0.38)		
	SR ver	-2.8(-7.83 1.98)	0.11(0.07 0.20)	0.16(0.15 0.17)	8.35(8.08 8.67)	0.92(0.84 0.96)
	MR ver	8.73(2.93 13.19)	0.12(0.06 0.20)	0.04(0.03 0.06)	21.1(17.43 26.59)	0.92(0.89 0.96)
	OR obl	-9.83(-13.15 -7.05)	0.64(0.43 0.86)	1.99(1.96 2.02)		
	SR obl	-3.75(-7.76 -0.44)	0.55(0.36 0.83)	0.87(0.86 0.89)	8.23(8.06 8.50)	0.92(0.84 0.96)
	MR obl	8.53(3.27 12.69)	0.52(0.26 0.81)	0.18(0.11 0.32)	24.36(18.39 28.90)	0.92(0.84 0.96)
	OR unip	-2.57(-5.83 -1.15)	0.92(0.74 1.04)	1.23(1.04 1.71)		
	SR unip	4.81(2.80 8.05)	0.85(0.71 0.98)	0.45(0.35 0.57)	11.58(7.77 13.72)	0.93(0.89 0.96)
	MR unip	6.79(5.05 10.87)	0.84(0.69 0.96)	0.36(0.24 0.45)	13.79(9.20 16.91)	0.96(0.92 0.96)

Table 2. Wilcoxon signed rank test results on the real dataset (significance threshold at $p < 0.05$, significant differences marked with*).

	SIR Results	Maternal Attenuation	Peak Detector Accuracy
SR hor vs MR hor	0.0009 *	0.0001 *	0.0043 *
SR ver vs MR ver	0.0003 *	0.0000 *	0.0009 *
SR obl vs MR obl	0.0008 *	0.0000 *	0.0000 *
SR unip vs MR unip	0.0006 *	0.0000 *	0.0001 *
SR vs MR	0.0000 *	0.0000 *	0.0000 *

Table 3. Wilcoxon signed rank test results on the synthetic dataset (significance threshold at $p < 0.05$, significant differences marked with*).

	SIR Results	Maternal Attenuation	Peak Detector Accuracy
SR hor vs MR hor	0.0000 *	0.0000 *	0.4514
SR ver vs MR ver	0.0000 *	0.0000 *	0.2055
SR obl vs MR obl	0.0000 *	0.0000 *	0.4115
SR unip vs MR unip	0.0002 *	0.0001 *	0.8280
SR vs MR	0.0000 *	0.0000 *	0.5800

Finally, the above results enable an analysis of the behavior of the SR implementation for the different leads. Widrow et al. [16] asserted that maternal attenuation strongly depends on the electrode placement. In our dataset, the horizontal lead was parallel to the maternal lead taken as reference for the SR implementation and the results in terms of the SIR and maternal attenuation were significantly better than those obtained from the vertical oblique leads and unipolar channel on the real dataset. It is important to emphasize that the SIRs on the raw traces were similar for the different leads, with only the oblique lead having a lower value due to the stronger mECG contribution to that lead (Figure 8), even though the fetal QRS amplitude was also higher. However, on the synthetic traces, the performance of the SR method on the horizontal abdominal lead were not significantly better than those achieved on the other leads. In particular, the results on the oblique lead outperformed the others. Again, this result should serve as a warning regarding the adoption of simulated signals for this kind of evaluation.

In general, in terms of output signal quality, even though the MR adaptive filter output was better than that of the SR, it seemed to suffer from residual noise as well as power-line interference. As such, a post-processing stage is called for, which was beyond the scope of this work. Figure 12 shows an example of the output signals without any post-processing.

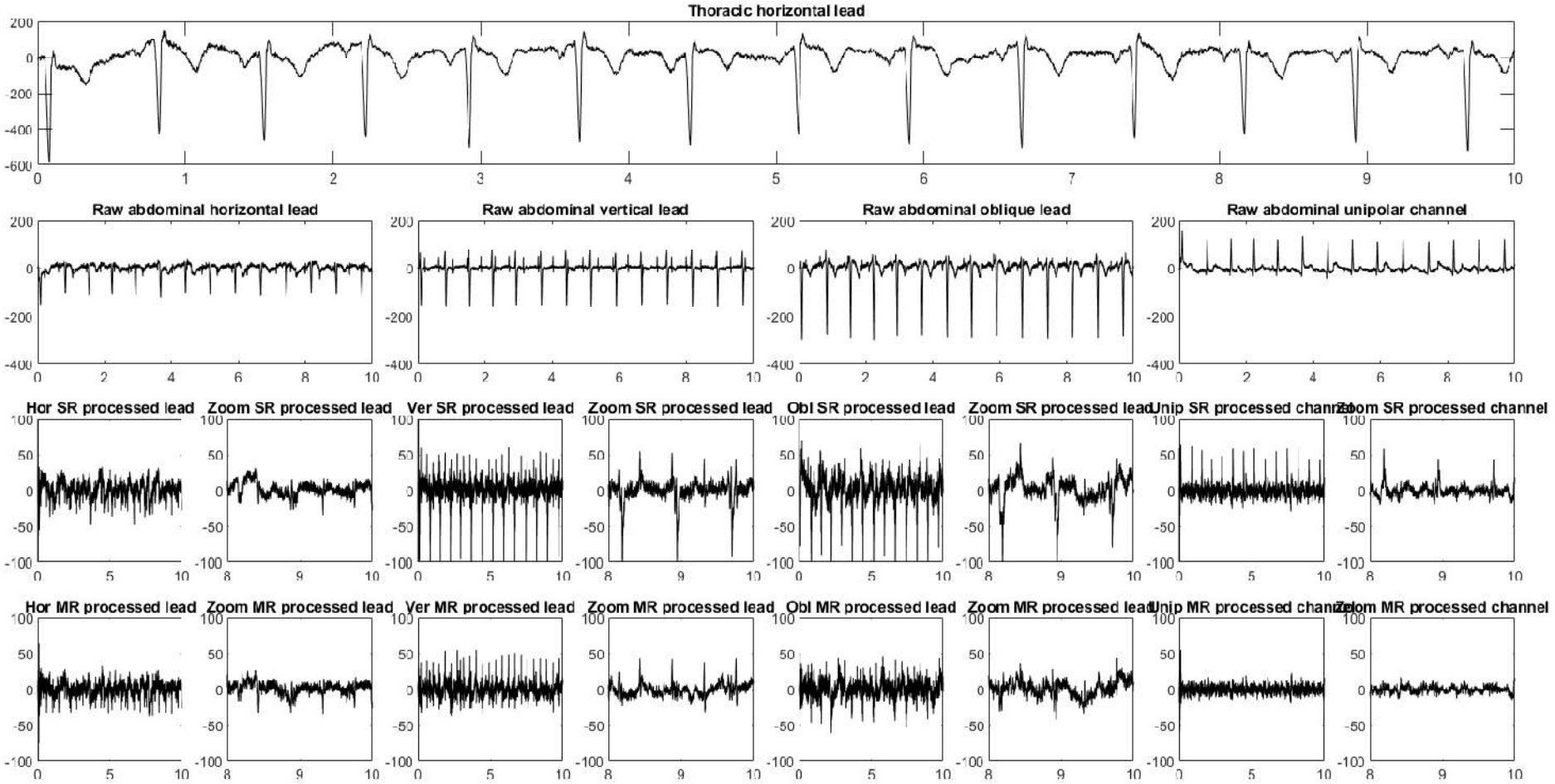

Figure 12. Real dataset: raw thoracic lead and raw and processed abdominal leads at different zoom levels for a single subject. In detail: (i) the first row shows the thoracic horizontal maternal lead used as reference in the SR implementation; (ii) in the second row, there are the four raw leads with the order: horizontal, vertical, and oblique leads and unipolar channel; (iii) in the third row, these signals are respectively processed using the SR method and each is plotted with its respective zoom; and (iv) the last row shows the signals processed by the MR technique and their zooms.

4. Conclusion

In this work, we systematically addressed the problem of the extraction of a fetal ECG from non-invasive recordings using QRD-RLS adaptive filters with single and multiple references. Since adaptive filters can be used when a reduced number of leads is needed to minimize setup complexity, especially in wearable applications, it is important to understand to what extent a SR adaptive filter can provide an adequate mECG attenuation that provides, at the least, a robust fetal QRS detection for fHR estimation. To this end, we tested SR and MR implementations of the same adaptive filter on real and synthetic signals and implemented up to three maternal thoracic references and four abdominal leads (three differential with 45 deg spacing, and one unipolar). The comparative analysis results confirmed the superiority of the MR as compared to the SR implementation ($p < 0.0000$) and the strong dependency of the latter on the electrode placement. Our quantitative results in terms of mECG attenuation and SIR values demonstrated how, by using multiple rather than single mECG reference leads even when dealing with a reference lead that is parallel to the abdominal lead, superior performance can always be achieved. Moreover, we found the accuracy of a fetal QRS detector applied to the output of the SR adaptive filter to be poor on real recordings (68% on average, $\sigma = 0.0097$). This means that SR approaches should be avoided in any case when trying to solve the non-invasive fECG extraction problem, even when the objective is to simply obtain the heart rate and even when a reference channel parallel to the abdominal channel is available. Overall, we can conclude that it is always worthwhile to use multiple rather than a single mECG reference lead when dealing with real non-invasive fECG recordings. It is also important to emphasize that the synthetic dataset in some cases led to results that were in direct contrast to the experimental evidence, which suggests that caution must be taken when using synthetic signals or, at least, in discussions of the results obtained by the algorithms for these datasets.

Secondly, the results of this study highlighted the better performance of differential measurements in enhancing the fECG amplitude, although they can also amplify the maternal interference, depending on the chosen abdominal lead. Finally, even the output of the best performing MR QRD-RLS algorithm seems to suffer from residual noise, beyond that of power-line interference, so we recommend the adoption of an ad-hoc denoising stage cascaded to the fECG extraction stage.

Acknowledgments

The authors wish to thank the team headed by Dr. Roberto Tumbarello, Division of Paediatric Cardiology, S. Michele Hospital (Cagliari, Italy), for the important support. We also wish to acknowledge all the involved voluntary pregnant women. Eleonora Sulas is grateful to Sardinia Regional Government for supporting her PhD scholarship (P.O.R. F.S.E., European Social Fund 2014–2020).

Conflict of interest

The authors declare no competing interests.

References

1. M. G. Signorini, A. Fanelli and G. Magenes, Monitoring fetal heart rate during pregnancy: Contributions from advanced signal processing and wearable technology, *Comput. Math. Methods Med.*, **2014** (2014).
2. American College of Obstetricians and Gynecologists, American college of obstetricians and gynecologists intrapartum fetal heart rate monitoring: Nomenclature, interpretation, and general management principles; ACOG practice bulletin no. 106, *Obstet. Gynecol.*, **114** (2009), 192–202.
3. M. Ferrario, M. G. Signorini and G. Magenes, Complexity analysis of the fetal heart rate variability: early identification of severe intrauterine growth-restricted fetuses, *Med. Biol. Eng. Comput.*, **47** (2009), 911–919.
4. D. Hoyer, J. Żebrowski, D. Cysarz, et al., Monitoring fetal maturation-objectives, techniques and indices of autonomic function, *Physiol. Meas.*, **38 (**2017), R61–R88.
5. U. Schneider, F. Bode, A. Schmidt, et al., Developmental milestones of the autonomic nervous system revealed via longitudinal monitoring of fetal heart rate variability, *PLoS One*, **13** (2018), 1–13.
6. R. Weber, D. Stambach and E. Jaeggi, Diagnosis and management of common fetal arrhythmias, *J Saudi Hear. Assoc.*, **23** (2011), 61–66.
7. M. T. Donofrio, A. J. Moon-Grady, L. K. Hornberger, et al., Diagnosis and treatment of fetal cardiac disease: A scientific statement from the american heart association, *Circulation*, **21** (2014), 2183–2242.
8. A. Sacco, J. Muglu, R. Navaratnarajah, et al., ST analysis for intrapartum fetal monitoring, *Obstet. Gynaecol.*, **17** (2015), 5–12.
9. A. Dessì, D. Pani and L. Raffo, An advanced algorithm for fetal heart rate estimation from non-invasive low electrode density recordings, *Physiol. Meas.*, **35** (2014), 1621.
10. T. F. Oostendorp, A. van Oosterom and H. W. Jongsma, Electrical properties of tissues involved in the conduction of foetal ECG, *Med. Biol. Eng. Comput.*, **27** (1989), 322–324.
11. R. Sameni and G. D. Clifford, A review of fetal ECG signal processing; issues and promising directions, *Open Pacing. Electrophysiol. Ther. J*, **3** (2010), 4–20.
12. V. Zarzoso and A. K. Nandi, Noninvasive fetal electrocardiogram extraction: Blind separation versus adaptive noise cancellation, *IEEE Trans. Biomed. Eng.*, **48** (2001), 12–18.
13. S. Muceli, D. Pani and L. Raffo, *Non-invasive real-time fetal ECG extraction – A block-on-line DSP implementation based on the JADE algorithm*, Proceedings of the 1st International Conference on Bio-inspired Systems and Signal Processing, **2** (2008), 458–463. Available from: https://iris.unica.it/handle/11584/107493.
14. D. Pani, S. Argiolas and L. Raffo, *A DSP algorithm and system for real-time fetal ECG extraction,* 2008 Computers in Cardiology, **35** (2008), 1065–1068. Available from: https://ieeexplore_ieee.gg363.site/abstract/document/4749229.
15. D. Pani, G. Barabino and L. Raffo, NInFEA: An embedded framework for the real-time evaluation of fetal ECG extraction algorithms, *Biomed. Tech.*, **58** (2013), 13–26.
16. B. Widrow and S. D. Stearns, *Adaptive Signal Processing*, Englewood Cliffs, NJ: Prentice-hall, 1985.

17. M. Shadaydeh, Y. Xiao and R. Ward, *Extraction of fetal ECG using adaptive volterra filters*, 2008 16th European Signal Processing Conference, (2008), 1–5. Available from: https://ieeexplore_ieee.gg363.site/abstract/document/7080365.
18. R. Martinek, R. Kahankova, H. Skutova, et al., *Adaptive signal processing techniques for extracting abdominal fetal electrocardiogram*, 2016 10th International Symposium on Communication Systems, Networks and Digital Signal Processing (CSNDSP), (2016), 1–6. Available from: https://ieeexplore_ieee.gg363.site/abstract/document/7573974.
19. R. Kahankova, R. Martinek and P. Bilik, *Fetal ECG extraction from abdominal ECG using RLS based adaptive algorithms*, 2017. 18th International Carpathian Control Conference, (2017), 337–342. Available from: https://ieeexplore_ieee.gg363.site/abstract/document/7970422.
20. J. Behar, A. Johnson, G. D. Clifford, et al., A comparison of single channel fetal ECG extraction methods, *Ann. Biomed. Eng.*, **42** (2014), 1340–1353.
21. S. Rajaguru and D. V. Prasad, A novel technique for extraction of FECG using multi stage adaptive filtering, *J. Appl. Sci.***, 10** (2010), 319–324.
22. S. Ravindrakumar and K. Bommannaraja, Certain investigation on De-noising the multichannel abdominal ECG signal using various adaptive noise suppression techniques, *Aust. J. Basic Appl. Sci.*, (2015), 372–380.
23. I. Silva, J. Behar, R. Sameni, et al., *Noninvasive cetal ECG: The physionet/computing in cardiology challenge 2013*, Computing in Cardiology 2013, **40** (2013), 149–152. Available from: https://ieeexplore_ieee.gg363.site/abstract/document/6712433.
24. R. Rodrigues, Fetal beat detection in abdominal ECG recordings: global and time adaptive approaches, *Physiol. Meas.*, **35** (2014), 1699–1711.
25. S. L. Lima-Herrera, C. Alvarado-Serrano and P. R. Hernández-Rodríguez, *Fetal ECG extraction based on adaptive filters and Wavelet Transform: Validation and application in fetal heart rate variability analysis*, 2016 13th International Conference on Electrical Engineering, Computing Science and Automatic Control (CCE), (2016), 1–6. Available from: https://ieeexplore_ieee.gg363.site/abstract/document/7751243.
26. J. Behar, F. Andreotti, S. Zaunseder, et al., An ECG simulator for generating maternal-foetal activity mixtures on abdominal ECG recordings, *Physiol. Meas.***, 35** (2014), 1537.
27. E. Sulas, E. Ortu, L. Raffo, et al., *Automatic recognition of complete atrioventricular activity in fetal pulsed-wave doppler signals*, 2018 40th Annual International Conference of the IEEE Engineering in Medicine and Biology Society (EMBC), **18** (2018), 917–920. Available from: https://ieeexplore_ieee.gg363.site/abstract/document/8512329.
28. F. Andreotti, J. Behar, S. Zaunseder, et al., An open-source framework for stress-testing non-invasive foetal ECG extraction algorithms, *Physiol. Meas.*, **37** (2016), 627–648.
29. A. H. Sayed, *Adaptive Filters*, John Wiley & Sons, 2011.
30. N. Chaitra, G. PraveenKumarY and M. Z. Kurian, Design and implementation of high performance adaptive FIR filter systems using QRD-RLS method, *Int. J. Adv. Res. Electr. Electron. Instrum. Eng.* **3** (2014), 2320–3765.
31. J. A. Apolinário and R. Rautmann, *QRD-RLS Adaptive Filtering*, Ed. José Antonio Apolinário, New York: Springer, 2009.
32. P. Kligfield, L. S. Gettes, J. J. Bailey, et al., Recommendations for the standardization and interpretation of the electrocardiogram: part I: The electrocardiogram and its technology a scientific statement from the american heart association electrocardiography and arrhythmias

committee, council on clinical cardiology; the american college of cardiology foundation; and the heart rhythm society endorsed by the international society for computerized electrocardiology, *J. Am. Coll. Cardiol.*, **49** (2007), 1109–1127.
33. J. Pan and W. J. Tompkins, A real-time QRS detection algorithm, *IEEE Trans. Biomed. Eng.*, **3** (1985), 230–236.
34. M. J. O. Taylor, M. J. Smith, M. Thomas, et al., Non-invasive fetal electrocardiography in singleton and multiple pregnancies, *BJOG*, **110** (2003), 668–678.
35. B. Surawicz, R. Childers, B. J. Deal, et al., AHA/ACCF/HRS Recommendations for the standardization and interpretation of the electrocardiogram, *J. Am. Coll. Cardiol.*, **119** (2009), e235–e240.
36. J. Behar, J. Oster and G. D. Clifford, Combining and benchmarking methods of foetal ECG extraction without maternal or scalp electrode data, *Physiol. Meas.*, **35** (2014), 1569–1589.
37. S. M. M. Martens, C. Rabotti, M. Mischi, et al., A robust fetal ECG detection method for abdominal recordings, *Physiol. Meas.*, **28** (2007), 373–388.

AIMS Press